Neutron emission in central heavy-ion collisions of ^{165}Ho + ^{20}Ne at 11, 14.6, and 20.1 MeV/nucleon

E. Holub,* D. Hilscher, G. Ingold, U. Jahnke, H. Orf, and H. Rossner
Hahn-Meitner-Institut für Kernforschung Berlin, 1000 Berlin 39, Federal Republic of Germany
(Received 26 January 1983)

The neutron emission from fusionlike reactions leading to evaporation residues and fission fragments was measured in the reaction ^{165}Ho + ^{20}Ne at 220, 292, and 402 MeV ^{20}Ne bombarding energies. Preequilibrium high-energy neutrons having up to twice the beam velocity were observed. The multiplicity of these neutrons increases with the bombarding energy from 0.4 to 2.3. This corresponds to 5 to 15 % of the total number of neutrons emitted per fusionlike event. The measured energy spectra of the highly energetic neutrons cannot be described with the Fermi-jet mechanism (one body promptly emitted particles), especially at angles larger than 35°. Reasonable agreement with the modified Harp-Miller-Berne model can be obtained. In that case, however, it is necessary to treat the initial degree of freedom as a parameter which increases with bombarding energy from 20 to 28. The evaporative component in the energy spectra of fusion-fission events was used to deduce that the number of prefission neutrons is 5.6±0.5, 5.8±0.5, and 5.3±1.0 at bombarding energies of 220, 292, and 402 MeV, respectively, whereas the statistical model predicts a maximum number of 1.6 to 2.0 prefission neutrons. Although no conclusive explanation can be given for the unexpectedly large multiple chance fission probability, it is suggested that most of the additional prefission neutrons are emitted during the transition from saddle to scission.

NUCLEAR REACTIONS ^{165}Ho + ^{20}Ne$\rightarrow A + n$, $E_{\text{lab-Ne}} = 220$, 292, and 402 MeV; A = evaporation residues or fusion-fission fragments; measured $\sigma(E_A,\theta_A,E_n,\theta_n)$ for $7.5° \leq \theta_n \leq 160°$, $6.5 \leq \theta_A \leq 60°$; deduced neutron multiplicities and energy spectra; prefission neutron multiplicities and temperatures.

I. INTRODUCTION

In heavy-ion collisions a large amount of kinetic energy can be dissipated into internal degrees of freedom.[1] The dissipation mechanisms are of crucial importance for our understanding of these reactions. The important knowledge in this respect is the time evolution of the conversion of initially available kinetic energy above the Coulomb barrier into internal degrees of freedom. This evolution we hope to deduce by means of the light-particle emission. A large amount of experimental information exists[2–10] for peripheral reactions, that is, for reactions in which the identity of projectile and target is essentially preserved. The analysis of light-particle emission in peripheral collisions is extremely complicated[5] since slow- and fast-moving sources are present which sequentially emit light particles. The light particles emitted from the fast moving fragment result in very high particle energies which will interfere with highly energetic particles emitted during the interaction time from the dinuclear system. However, our main interest concerns just those light particles because they will tell us about the early stages of the energy dissipation. In many studies of light-particle emission in heavy-ion collisions the question of whether or not the measured high-energy light particles originate from a true preequilibrium process or from a sequential decay could not uniquely be resolved, and in some cases[7–10] erroneous results were obtained. The situation is considerably easier for central collisions leading to fusionlike reactions. In this case there exist only one or two slowly moving fragments if the compound nucleus survives as an evaporation residue or fissions, respectively.

Many models which predict high-energy particles in heavy-ion collisions have been proposed. We will compare our experimental results with the modified Harp-Miller-Berne[11] and the Fermi-jet models only.[12] The exciton model will enable us to make a link to light-ion induced reactions. This will lead us

to the important question of whether or not heavy-ion collisions indeed result in new phenomena not encountered in the much simpler environment of light-ion induced reactions. The second model we will discuss is the Fermi-jet model which basically relates the high-energy particles with the Fermi velocity in nuclei. Since this velocity, however, is tied to the nuclear density, the Fermi-jet mechanism would enable us to probe the nuclear density. This indeed would be a characteristic new phenomenon which we can study only in heavy ion collisions.

However, not only the light particles emitted prior to reaching equilibrium are of interest, but, also, the evaporated particles can yield a major contribution to our understanding of level densities at various deformations, temperature dependent transmission coefficients, etc. Furthermore, one can use the evaporation of light particles as a clock to measure the lifetime of the composite nucleus prior to fission. To this purpose we use the number of neutrons emitted prior to and after fission. Owing to the large number of neutrons, the emission of which is not hindered by the Coulomb barrier we can study the question: How do high temperatures and angular momenta influence the fission lifetime, and, in particular, how do fission and particle emission compete? For angular momenta larger than the angular momentum J ($B_f=0$) at which the fission barrier vanishes one might expect very short fission lifetimes.[13] Recently Gavron *et al.*[14] have measured in the system ^{150}Nd + ^{20}Ne quite long fission lifetimes also for $J > J$ ($B_f=0$). The neutron evaporation prior to and after fission thus can be used to study fission dynamics.

II. EXPERIMENTAL PROCEDURE

The experiments were performed at the VICKSI accelerator of the Hahn-Meitner-Institute in Berlin. Neutron emission was studied in the reaction ^{165}Ho + ^{20}Ne at 220, 292, and 402 MeV ^{20}Ne bombarding energies, corresponding to 6.5, 10.1, and 15.5 MeV/nucleon of relative motion above the Coulomb barrier, respectively. Self-supporting ^{165}Ho targets were used with thicknesses ranging from 400 to 490 μg/cm^2. A schematic setup of the experiment at 220 MeV bombarding energy is shown in Fig. 1. The scattering chamber was made of 3 mm thick steel, with a diameter of 1 m. The beam was dumped 5.4 m downstream from the target in a graphite Faraday cup shielded by a specially designed iron, lead, and paraffin beam dump (BD) with a diameter of 2 m.

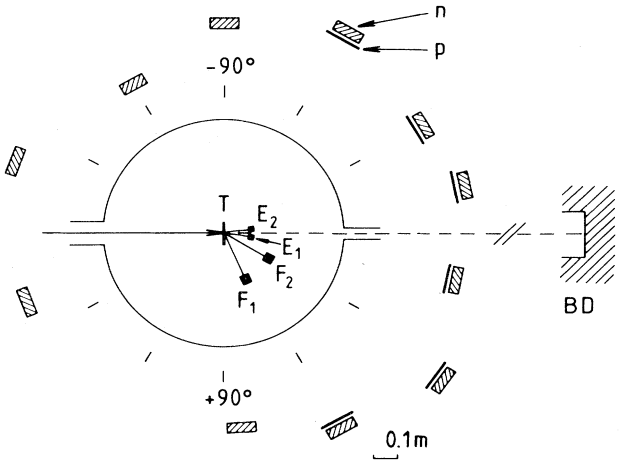

FIG. 1. Schematic diagram of the experimental setup for the experiment at the 220 MeV bombarding energy.

A. Heavy-ion detectors

Projectilelike (PL), fusion-fission fragments (FF) and evaporation residues (ER) were identified by measuring their energy and time of flight. The energy was measured with solid-state detectors. The setup for the experiment at 220 MeV consisted of two 500 μm thick silicon surface-barrier detectors, E_1 and E_2, detecting the evaporation residues and the fusion-fission fragments. They were placed symmetrically on each side of the beam axis at $\pm 8°$ and $\pm 19°$. The distance from the target and the detector aperture were ≈ 10 cm and 2.2 mm ϕ, respectively. The FF fragments at larger angles were detected in 60 μm thick silicon fission detectors, placed at $+65°$ (F_1) and $+30°$ (F_2). The distance from the target was ≈ 19.5 cm; the detector aperture was 20 mm ϕ.

The setup for the experiments performed at 292 and 402 MeV bombarding energies was somewhat different. It consisted of one ΔE-E solid-state telescope (TEL), since in these experiments we were also studying peripheral collisions leading to PL fragments. The telescope system was comprised of a 50 μm thick ΔE detector and a 500 μm thick E detector. The system was used for charge and mass identification of PL fragments, whereas the ER and FF products were identified by means of their energy and time of flight. The telescope was placed at ≈ 10 cm from the target at $-10°$ (402 MeV), and $-16°$, $-22°$ (292 MeV). The subtended solid angle was 3.5 msr. The FF fragments were additionally detected in a 60 μm thick fission detector, placed at $+60°$ and $+40°$ in the experiment at 292 MeV, and at $+57°$ in the 402 MeV experiment. At all three

bombarding energies the angle $\theta_{FF} \approx 60°$ was chosen in such a way that the correlated, undetected symmetric fission fragment was emitted to $-\theta_{FF}$, i.e., symmetric to the beam direction.

The time of flight of heavy ions was measured relative to the beam bunches of the cyclotron with a time separation between two bunches of approximately 60 ns. For heavy-ion detection a typical energy resolution was 1 MeV and the time resolution was 0.5 ns FWHM for the elastic peak.

The separation of different reaction products was done according to their masses and velocities, determined by the energy and the flight time. A two-dimensional plot of heavy-ion flight time vs heavy-ion energy for the experiment at a bombarding energy of 292 is shown in Fig. 2. The heavy residues (HR), FF, and PL products are well separated. In order to distinguish between targetlike recoils (TR) due to deep inelastic reactions or incomplete fusion and ER due to almost complete momentum transfer, we employed the measured velocity distributions. These distributions are characterized by a Gaussian distribution centered at the velocity corresponding to almost complete momentum transfer, and a low-velocity tail which is due to target recoils. The relative intensity of the latter component is increasing with angle (Fig. 3). To ensure that the neutron coincidences were not contaminated with neutrons from TR, that is, more peripheral collisions, the low-velocity tail was cut off for the coincidence data (see Sec. III A).

B. Neutron detectors

Neutrons, in coincidence with PL, ER, and FF products were detected with NE-213 liquid scintillators, which were 2.5 or 5.1 cm thick and had a diameter of 12.7 cm. Neutrons were detected at 11 angles in plane and at one angle (85°) out of plane. The angles and distances of neutron detectors together with the positions of heavy-ion detectors in all three experiments are given in Table I. In connection with the neutron detectors highly efficient

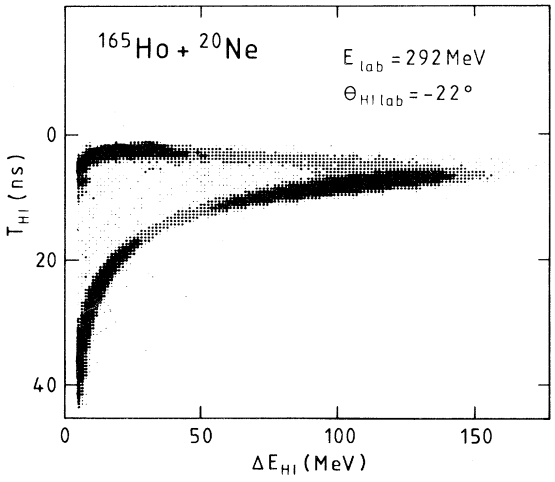

FIG. 2. Two-dimensional plot of the heavy-ion flight-time (T_{HI}) vs energy loss (ΔE_{HI}) in a 50 μm thick detector.

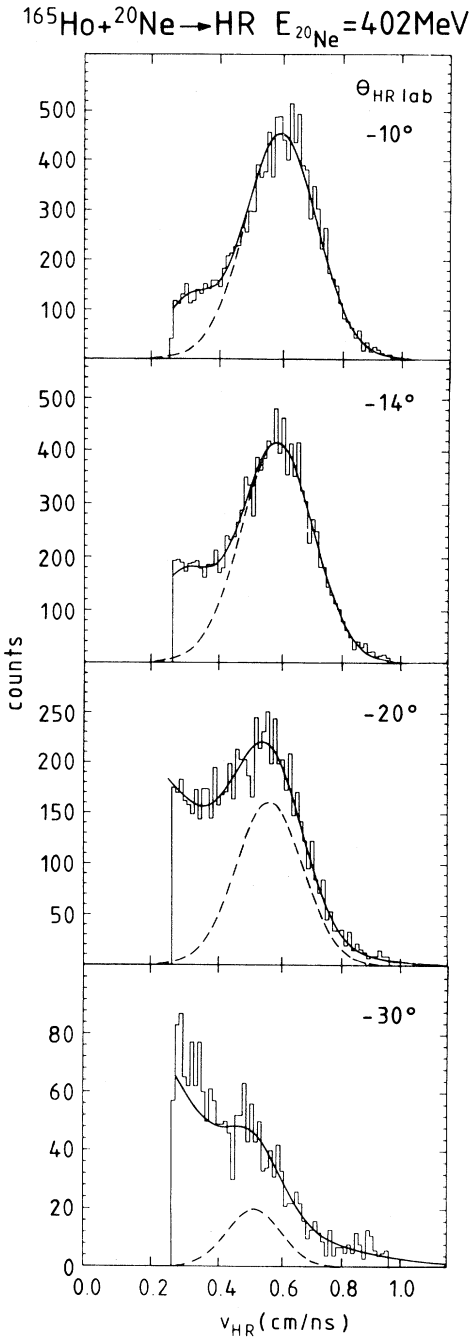

FIG. 3. Velocity distribution of heavy residues. The cutoff at 0.25 cm/ns is caused by an experimental threshold.

TABLE I. Neutron-detector positions and the position of heavy-ion detectors in the experiments at the 220, 292, and 402 MeV ^{20}Ne bombarding energies.

^{20}Ne bombarding energy							
220 MeV		292 MeV				402 MeV	
$\theta_{E_1}=+9.5°$	$\theta_{E_2}=-6.5°$	$\theta_{\mathrm{TEL}}=-16°$		$\theta_{\mathrm{TEL}}=-22°$		$\theta_{\mathrm{TEL}}=-10°$	
$\theta_{\mathrm{FF}_1}=65°$	$\theta_{\mathrm{FF}_2}=30°$	$\theta_{\mathrm{FF}}=60°$		$\theta_{\mathrm{FF}}=40°$		$\theta_{\mathrm{FF}}=57°$	
$\theta_{n\,\mathrm{lab}}$ (deg)	l_n (cm)	$\theta_{n\,\mathrm{lab}}$ (deg)	l_n (cm)	$\theta_{n\,\mathrm{lab}}$ (deg)	l_n (cm)	$\theta_{n\,\mathrm{lab}}$ (deg)	l_n (cm)
−12.5	107.5	−15.0	94.7	−7.5	169.0	−8	104.9
−30.0	92.9	−35.0	94.7	−70.0	94.5	−30	76.6
−60.0	102.0	−70.0	94.5	−118.0	94.5	−60	89.1
−90.0	90.1	−90.0	94.5	8.0	154.8	−85	71.7
−120.0	74.3	−118.0	94.5	25.0	97.4	−120	57.9
−160.0	90.4	−155.0	94.5	80.0	94.5	−160	70.0
12.5	96.6	8.0	154.8			8	91.1
35.0	109.7	15.0	95.0			30	77.0
60.0	96.7	35.0	94.9			60	88.8
85.0	83.6	60.0	94.9			85	69.1
160.0	85.9	80.0	94.5			120	60.0
85.0[a]	92.1	105.0	94.5			85[a]	86.1

[a]Out-of-plane position.

γ-n pulse-shape discriminator circuits were employed to distinguish neutrons from γ rays.

The neutron energy was determined with a time-of-flight method. The time delay between an event in the heavy-ion detector and one in a neutron detector was measured. This time was, event by event, added to the flight time of the heavy ion, resulting in the neutron time of flight. The overall time resolution achieved for γ rays was typically 1 ns FWHM. This time resolution results in energy resolutions of 0.3, 1, and 11 MeV for neutron energies of 5, 10, and 50 MeV, respectively, for a flight path of 1 m. A scatter plot of the neutron time of flight versus the heavy-ion time of flight is shown in Fig. 4 for the experiment at the 402 MeV bombarding energy. Neutrons and γ rays are well separated. Furthermore, we observe neutrons in three subgroups corresponding to coincidences with HR, FF, and PL products. Since for each fragment type (HR, FF, and PL) time zero was determined via the γ-ray time of flight, the measured neutron time of flight is independent of the plasma delay time[20] in the heavy-ion detector.

Figure 5 shows measured time-of-flight spectra for neutrons and γ rays in coincidence with ER ($\theta_{\mathrm{ER}}=-10°$) for the experiment at the 402 MeV bombarding energy. The neutron detector was at $\theta_{n\,\mathrm{lab}}=-8°$, and the electronic neutron threshold was 0.84 MeV. This figure displays the scatter plots of the recoil energy for neutrons and γ rays versus the time of flight. The respective projections on the time-of-flight axis are also shown. It is evident that, without n-γ discrimination, γ rays would contaminate the high-energy neutron spectrum, even at recoil energies larger than 2 MeV. The small, narrow peak in the projection of the neutron time-of-flight spectrum, appearing at $t_n \approx 16$ ns is due to γ rays not rejected by the pulse-shape discrimination system. These events are rejected off line from the

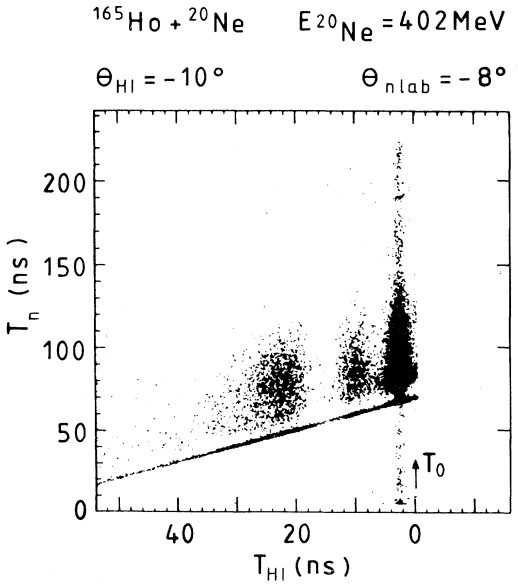

FIG. 4. Scatter plot of the neutron time of flight (T_n) vs the heavy-ion time of flight (T_{HI}).

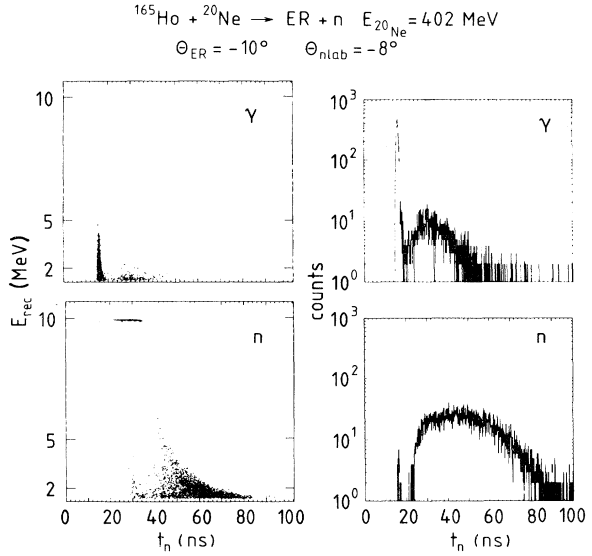

FIG. 5. Scatter plot of the recoil energy in a NE-213 scintillator for neutrons and γ rays vs neutron time of flight and the respective projection on the neutron time-of-flight axis.

time-of-flight spectrum.

The neutron detection efficiencies were calculated for both neutron detector sizes with a Monte Carlo code from Cecil *et al.*[15] for neutron energies up to 300 MeV. The results of this code agree within a few percent with the results of the code of Textor *et al.*[16] for neutron energies below 50 MeV and the measured efficiencies of Drosg *et al.*[17] The detector efficiency depends strongly on the threshold set for the proton-recoil energy. The energy calibration was done using the Compton-edge energies of various radioactive γ-ray sources. The hardware neutron threshold was set between 0.7 and 1.10 MeV equivalent neutron energy.[18] Additionally, to decrease the background, the thresholds were increased off-line to values of 1.3 to 2 MeV. In order to check the spectra at high neutron energies, thresholds of 5 and 10 MeV were applied.

The accuracy of the neutron detection system, the calibrations and the efficiencies were tested by detecting neutrons from ^{252}Cf fission fragments. The neutron-detection geometry was the same as during the experiment with heavy ions. Measured neutron spectra were compared with the results of Bowman *et al.*[19] The agreement was in general better than 10%. Additional corrections were needed only for low-energy neutrons ($E_n \leq 3$ MeV) detected behind the heavy-ion detector. These shielding effects were corrected by using the ^{252}Cf calibration measurements.

In order to deduce the differential neutron multiplicity spectra, the number of neutrons detected in coincidence with ER, FF, and PL products was normalized to the total number of single ER, FF, and PL events. In the experiment at the 292 MeV bombarding energy single heavy-ion events were counted together with neutron coincidences. In the 220 and 402 MeV experiments neutron coincidence runs were normalized to single runs which were performed separately before and after each coincidence run.

High-energy charged particles may penetrate the 3 mm thick steel wall of the scattering chamber and the scintillator housing. For protons this energy should be greater than 35 MeV. In order to reject those particles, 2 mm thick, 15.5 cm$\times$15.5 cm NE-104 plastic scintillator paddles (denoted by *p* in Fig. 1), were placed in front of the forward neutron detectors. They were used in anticoincidence to the neutron detectors. The reduction of neutron flux by these 2 mm thin paddles was smaller than 2%. All scintillators without proton paddles were covered with 2 mm thick lead caps in order to suppress low-energy γ rays and atomic x rays.

C. Data aquisition

The following parameters were written event by event on disk: (i) heavy-ion detector: energy E_{HI}, energy loss ΔE_{HI}, and time of flight T_{HI}; (ii) neutron detector: scintillator light output L_n, time of flight T_n, and a neutron or γ bit deduced from the n-γ pulse-shape discrimination unit; (iii) proton paddle: scintillator light output L_p and time of flight T_p. Owing to limitations of the data acquisition system six neutron detectors were always mixed into one parameter, and an identification bit was set for each detector. If out of these six detectors more than one detector fired, a special rejection bit was set. This enabled us to correct for all rejected events ($<1\%$). Similarly, the six proton paddles and two heavy-ion detectors were mixed and tagged with route bits.

III. DATA ANALYSIS AND RESULTS

A. Neutrons in coincidence with evaporation residues

The HR are not necessarily ER, but can also be contaminated by TR due to massive transfer reactions. Therefore, it is necessary to measure neutrons in coincidence with ER only at the most forward direction and, in addition, to gate the neutrons with the high-velocity part of HR. For experiments at 220, 292, and 402 MeV the HR products having velocities $V_{HR} \geq 0.27$, 0.36, and 0.38 cm/ns, respectively, have been considered as ER. The mean V_{ER}

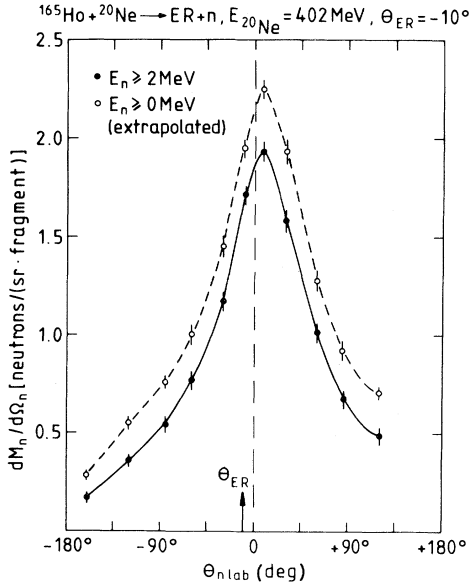

FIG. 6. The experimental angular correlation of neutron multiplicities measured in coincidence with ER at the 402 MeV bombarding energy for neutrons with energy $E_n \geq 2$ MeV (filled circles). Open circles denote the respective values extrapolated to neutron energies smaller than 2 MeV. The solid and dashed lines are drawn through the data points.

velocities at these three bombarding energies were 0.45 (220 MeV), 0.54 (292 MeV), and 0.60 cm/ns (402 MeV). The respective velocities corresponding to full momentum transfer would correspond to 0.50, 0.57, and 0.67 cm/ns, respectively. The experimental absolute values are, however, uncertain to $\approx 10\%$, since we do not know exactly the plasma delay[20] of the ER which is assumed to be 1.5 ns. The main criterion was not the absolute velocity but rather the shape of the velocity spectrum.

A second important effect to be discussed is the left-right asymmetry in the neutron angular correlation. Neglecting the recoil of the detected neutron imparted to the ER we expect an angular correlation symmetric with respect to the ER detection angle (θ_{ER}). In reality, however, the detection of one neutron emitted from the ER introduces a shift of the mean detection angle of the recoiling ER. Owing to the strongly forward peaked angular distribution of ER the maximum of the angular correlation is shifted towards the beam or, as in our case, even to the other side of the beam. In Fig. 6 we show the experimental neutron multiplicity angular correlation measured at 402 MeV with $\theta_{ER} = -10°$, integrated over neutron energies $E_n \geq 2$ MeV (full circles). The asymmetry effect, introduced by the neutron recoil, is obvious. We also extrapolated the experimental neutron spectra to energies smaller than the experimental threshold in order to obtain an estimate for the total neutron multiplicity. The extrapolation was done using a Maxwellian shape of neutron spectra at small energies. The total number of neutrons in coincidence with ER was 11.4 ± 0.3. The corresponding results for 220 and 292 MeV were 7.3 ± 0.3 and 9.6 ± 0.3, respectively. The above mentioned recoil effect influences also the shape of the neutron energy spectra and, consequently, has to be taken into account when the temperature of the compound nucleus is extracted from these spectra. There are two possibilities to correct for the mentioned asymmetry effects. Neutron spectra, measured in coincidence with one ER detector, can be averaged over symmetric neutron angles left and right from the beam axis. A second possibility is to detect ER at two angles, symmetric to the beam axis, and average the neutron spectra measured at a given angle over these two symmetric ER angles. We performed both kinds of corrections. The data at 292 and 402 MeV were obtained with only one ER detector, and were averaged over neutron angles left and right from the beam axis. The data at 220 MeV were measured with two ER detectors placed at $\theta_{ER} = +9.5°$ and $-6.5°$. Both methods yielded equal results.

In Fig. 7 we show the averaged energy spectra of neutrons emitted in coincidence with ER at all three bombarding energies. All these spectra show the existence of two components. The low-energy component is predominantly due to evaporation from the compound nucleus. From this part of the neutron spectrum we can determine the temperature of the compound nucleus. The high-energy component is ascribed to preequilibrium emission. In order to obtain the temperature of the compound nucleus the energy spectra were fitted with the usual spectral shape for evaporation. In order to parametrize simultaneously neutron energy spectra at all angles and all neutron energies we assume that the high-energy preequilibrium component can also be described by a thermal source moving with a certain velocity. The exponential decrease of this component corresponds to a certain "temperature" of the emitting source. Therefore, we fitted the whole neutron energy region with a spectral shape given by[21]

$$\frac{d^2M_n(\theta_n)}{dE_n d\Omega_n} = \sum_{i=1}^{2} \frac{M_i \sqrt{E_n}}{2(\pi T_i)^{3/2}} \exp\left[-\frac{E_n - 2\sqrt{\epsilon_i E_n}\cos(\theta_i - \theta_n) + \epsilon_i}{T_i} \right] . \quad (1)$$

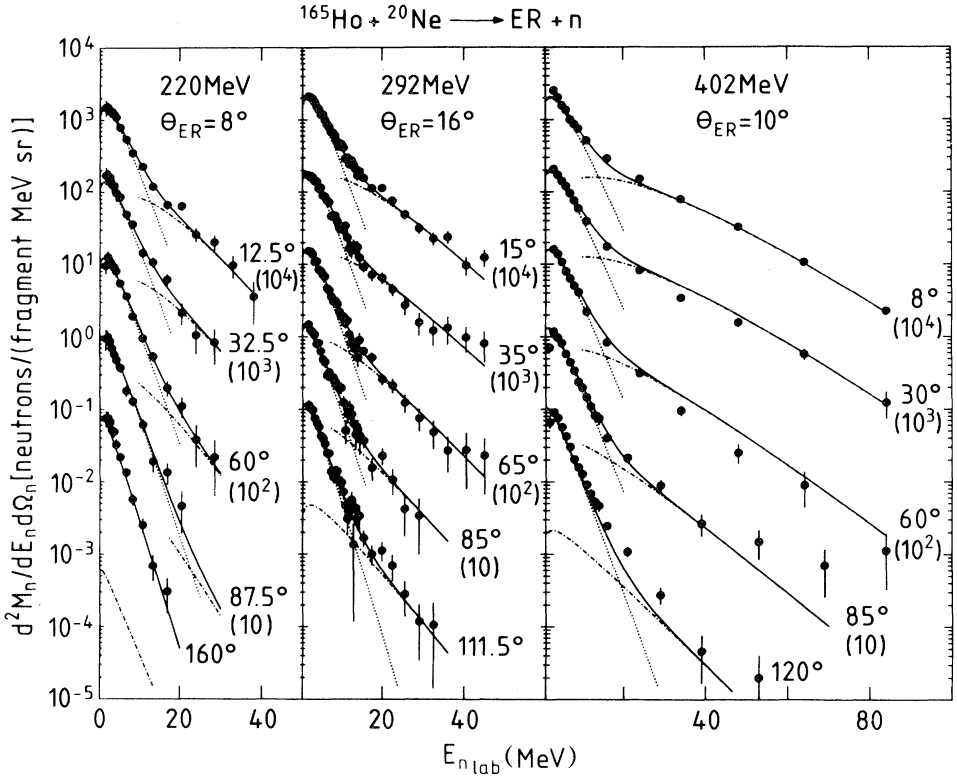

FIG. 7. Experimental differential neutron multiplicities in coincidence with ER at 220, 292, and 402 MeV bombarding energies (data points). The full curve represents the sum of the evaporative (dotted line) and preequilibrium components (dashed-dotted line). The curves were calculated using Eq. (1) and the parameters given in Table II.

The running index i denotes the two sources which contribute to neutron emission: evaporation from compound nucleus (EV) and preequilibrium emission (PE). The parameters M_i, E_n, and θ_n are neutron multiplicity, energy, and angle, respectively, while T_i, ϵ_i, and θ_i are nuclear temperature, energy per nucleon, and angle of the emitting neutron source. The energy per nucleon for the EV component is taken from the center-of-mass motion of the compound nucleus. The angles θ_i for both sources were taken to be 0°. Neutron spectra were fitted with Eq. (1) using M_{EV}, T_{EV}, M_{PE}, T_{PE}, and ϵ_{PE} as free parameters. In Table II we give the results obtained for the EV and PE components at all three bombarding energies. The given error bars correspond to an increase of the χ^2 value of about 10% above its minimal value. The calculated neutron spectra using Eq. (1) and the parameters given in Table II are shown with full lines in Fig. 7. We find a good agreement between the experimental spectra and the spectral shape (1). The best χ^2/point values are also given in Table II. An effective temperature for a neutron cascade can be calculated[22] from

$$T=\tfrac{11}{12}(E^*/a)^{1/2}\ ,$$

TABLE II. Parameters obtained by the least-squares fit of the neutron energy spectra in coincidence with evaporation residues.

			EV		PE			
E_{NE} (MeV)	E^*_{CN} (MeV)	$\frac{E_{\mathrm{c.m.}}-V_{\mathrm{CB}}}{\mu}$ (MeV/nucleon)	M_{EV} (neutrons)	T_{EV} (MeV)	M_{PE} (neutrons)	T_{PE} (MeV)	ϵ_{PE} (MeV/nucleon)	χ^2/point
220	165	6.5	6.7±0.5	2.4±0.2	0.4±0.1	4.5±0.3	3.8±0.3	0.8
292	229	10.1	8.4±0.6	2.3±0.2	1.4±0.2	6.3±0.3	2.1±0.4	0.9
402	325	15.5	10.1±0.6	2.8±0.2	1.5±0.2	8.6±0.3	5.6±0.4	1.7

where E^* is the initial excitation energy, and a is the level-density parameter. Using the level-density parameter

$$a=(A_p+A_T)/8$$

and $E^*=E^*_{\mathrm{CN}}$ (maximum excitation energy of the compound nucleus, Table II) we obtain effective temperatures of 2.4, 2.8, and 3.4 MeV at the bombarding energies of 220, 292, and 402 MeV, respectively.

The results for T_{EV} obtained by fitting the experimental data show that T_{EV} agrees with the calculated effective temperature at the lowest bombarding energy of 220 MeV, where only 0.4 ± 0.1 neutrons were emitted by the PE process. As the bombarding energy increases, T_{EV} becomes smaller than the calculated effective temperature by about 20%. One reason for this disagreement can be the preequilibrium emission increasing with bombarding energy. The least-squares fit analysis of neutron energy spectra shows that it is also possible to parametrize the high-energy tails of neutron spectra, using the spectral shape (1).

We note that the exponential slope of the high-energy neutron spectra at various angles can be simultaneously reproduced at the given bombarding energy with unique values T_{PE} and ϵ_{PE}. The "temperature" T_{PE} is considerably higher than T_{EV}, and ϵ_{PE} corresponds approximately to half the beam velocity. The mean number of preequilibrium neutrons, M_{PE}, obtained by this parametrization is a model-dependent quantity since we extrapolate the high energetic component to low neutron energies into the evaporative part of the spectrum assuming a spectral shape given by Eq. (1). A more detailed discussion of the preequilibrium part of the spectra will be given after we present the neutron spectra measured in coincidence with FF products.

B. Neutrons in coincidence with fusion-fission products

As is shown in Table I, at each bombarding energy neutrons were detected in coincidence with one FF product, emitted at various angles ranging from the forward direction ($\theta_{F_1}=6.5°$) to the symmetric-angle configuration $\theta_{F_1}\approx 60°$.

The fission of ^{165}Ho + ^{20}Ne proceeds, in the case of complete fusion, through the formation of the compound nucleus ^{185}Ir, which has a rather low fissility parameter of $x=0.66$. Already, at the lowest bombarding energy of 220 MeV, the critical angular momentum for fusion of ^{165}Ho + ^{20}Ne has reached its saturation value,[23] determined as $\approx 95\hbar$. On the other hand, the angular momentum at which the fission barrier vanishes[24] is $\approx 80\hbar$, i.e., $l_{Bf=0}<l^{\mathrm{FUS}}_{\mathrm{crit}}$. According to the measured σ_{ER}, the lowest angular momenta contributing to FF are between $58\hbar$ and $64\hbar$ for the three bombarding energies.

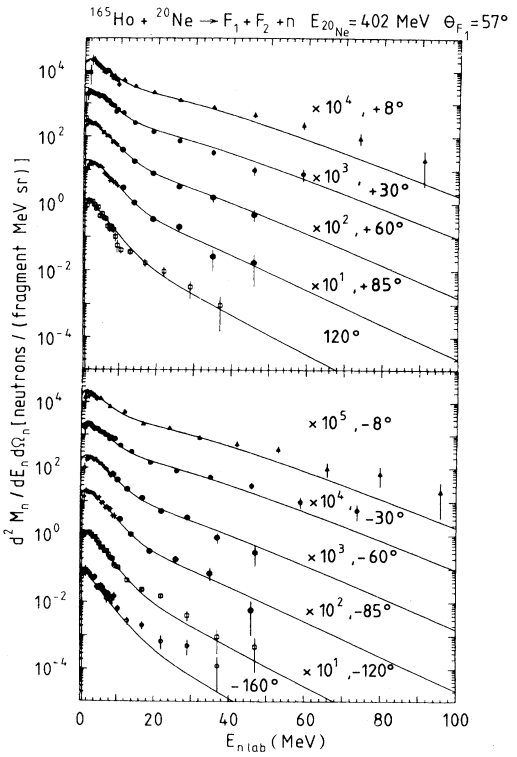

FIG. 8. Experimental differential neutron multiplicities in coincidence with one FF fragment detected at 57° and the 402 MeV bombarding energy (data points). Solid lines were calculated using Eq. (1) with the parameters given in Table III.

In Fig. 8 we show the neutron energy spectra measured at various angles in coincidence with one FF fragment detected at $\theta_{F_1}=57°$ and at the 402 MeV bombarding energy. The experimental spectra show again the low-energy component, due to evaporation, and the high-energy component, due to preequilibrium emission. The maximum laboratory energy of emitted neutrons decreases with increasing neutron angle ($\theta_{n\,\mathrm{lab}}$) and the slope of the measured high-energy tails becomes gradually steeper as θ_n increases.

In order to parametrize the experimental neutron spectra, we can again apply the multiple-source least-squares fit analysis of the experimental data, using the spectral shape given by Eq. (1). In the case of neutrons emitted in coincidence with FF fragments, the following components are expected to contribute to the neutron spectra: (i) preequilibrium emission, (ii) evaporation from the composite system before fission, and (iii) evaporation from each of the

two fission fragments.

We expect, therefore, three evaporation sources which determine the low-energy neutron emission, and one preequilibrium source producing mostly the high-energy neutrons. We will again assume that also the high-energy neutron spectra can be parametrized by a spectral shape determined by a source moving with a certain velocity $\propto$(energy/nucleon)$^{1/2}$ and characterized by a certain "temperature." From all parameters entering Eq. (1) with four sources, we take as known the energy/nucleon and the emission angle of the composite system and both fusion-fission fragments. The energy/nucleon of the composite system is taken to be that of the completely fused system, moving at 0°. The energy/nucleon of both FF fragments and the emission angle of the undetected FF product is calculated by assuming complete fusion and symmetric fission. The temperatures and the multiplicities for the evaporation from the composite system and both FF fragments, as well as the temperature, the multiplicity, and the energy/nucleon for the preequilibrium emission were taken as free parameters, determined by the least-squares fit to the experimental neutron energy spectra. The laboratory spectra were fitted simultaneously at all angles in the reaction plane. For the neutron evaporation from symmetric fission we assumed that $M_{F_1}=M_{F_2}$ and $T_{F_1}=T_{F_1}$, i.e., an equal number of emitted EV neutrons and equal temperatures for both FF fragments. The evaporation from the composite system and from both FF fragments will be called, respectively, the prefission and postfission emissions. The parameters obtained by fitting the data for the symmetric-fission configuration, also describe very well the measured neutron spectra at any other trigger angle, i.e., at $\theta_{F_1}=30°$, 40°, $-22°$, and $-10°$ (see Table I). Furthermore, we were able to reproduce with the same parameters also the neutron-FF coincidence data measured at out-of-plane neutron angles.

In Table III we summarize the results obtained for the free parameters by the least-squares fit analysis of neutron spectra in coincidence with one FF fragment at all three bombarding energies. The average χ^2/point values obtained for neutron spectra in coincidence with FF fragments detected at various θ_{FF} angles are also given in Table III. The error bars correspond to $\approx$10% higher χ^2 values than the best ones. The postfission EV neutron multiplicities in Table III are the sum of both FF fragments. The full lines in Fig. 8 represent the fit to the experimental differential neutron multiplicities obtained with the parameters given in Table III.

The present experimental data cover a wide range

TABLE III. Parameters obtained by the least-squares fit of the neutron energy spectra in coincidence with FF fragments.

			EV				PE			
			M_{EV} (neutrons)		T_{EV} (MeV)					
E_{Ne} (MeV)	E^*_{CN} (MeV)	$\frac{E_{c.m.}-V_{CB}}{\mu}$ (MeV/nucleon)	prefission	postfission	prefission	postfission	M_{PE} (neutrons)	T_{PE} (MeV)	ϵ_{PE} (MeV/nucleon)	χ^2/point
220	165	6.5	5.6±0.5	3.7±0.7	2.6±0.3	1.5±0.3	0.4±0.1	5.9±0.3	2.6±0.2	1.0
292	229	10.1	5.8±0.5	4.8±0.7	2.9±0.4	1.4±0.3	1.0±0.3	6.3±0.3	3.4±0.5	0.7
402	325	15.5	5.3±1.0	5.4±1.0	2.9±0.4	1.7±0.3	2.3±0.2	7.7±0.3	3.5±0.5	1.4
402	325	15.5	(6.1±1.0)	(6.8±1.0)	(3.3±0.4)	(2.1±0.3)				

of maximum available excitation energies from 165 to 325 MeV, though the system does not necessarily dissipate all this energy into internal excitation energy. The results for the evaporation part of the neutron spectra given in Table III show that, independent of excitation energy, the number of prefission neutrons is quite large and remains approximately constant, 5.6 ± 0.7 neutrons. The number of postfission neutrons increases gradually with bombarding energy. Furthermore, as a consequence of the high prefission neutron multiplicity, the temperature at the moment of fission is considerably lower than the temperature of the composite system prior to particle evaporation. The prefission temperatures are close to the temperatures expected from the excitation energy brought into the system for 220 and 292 MeV bombarding energies, but smaller for the highest bombarding energy of 402 MeV. The global dependence upon the bombarding energy of the fit parameters for the PE component of neutron spectra in coincidence with FF fragments is similar to that obtained by the analysis of the neutron-ER coincidence data (see Table II). The parameters M_{PE}, T_{PE}, and ϵ_{PE} increase as the bombarding energy increases. More detailed discussion of the results obtained for the PE emission of neutrons in coincidence with both products of central $^{165}\mathrm{Ho}+{}^{20}\mathrm{Ne}$ collisions (ER and FF fragments) will be given in Sec. IV B.

At this point we will discuss the results obtained for the prefission and postfission evaporation neutron emission. We wanted to check the sensitivity of the least-squares fit analysis method, applied to the evaporation part of the neutron spectra in coincidence with one FF fragment. For this purpose the iterative event-by-event method[21] was applied to the 402 MeV data. The results are also shown in Table III in the last line in parentheses. Within the error limits, these results agree with values obtained by the least-squares fit method.

In Fig. 9 we show the experimental differential neutron multiplicities ($E_n \leq 50$ MeV) in coincidence with one FF fragment at the 220 and 402 MeV bombarding energies, together with the calculations using Eq. (1) and the parameters given in Table III. We see that the forward and the backward evaporative neutron spectra are mostly described by the prefission contribution (dashed line). The neutron spectrum behind the detected fission fragment ($\theta_n = 60°$) is dominated by the postfission evaporation (dotted line). The preequilibrium component (dashed-dotted line) becomes very small at backward angles, but it is important at forward angles. Figure 10(a) shows the experimental angular correlation for neutrons having energies between 2 and 10 MeV at 402 MeV and $\theta_{F_1} = 57°$ together with the corresponding calculations obtained by the least-squares fit method. We see how each of the three components determines the neutron yield at various angles. In Fig. 10(b) the same parameters were used to calculate the angular correlation at another trigger angle $\theta_{F_1} = -10°$. Although the angular dependence of the n yield has completely changed due to the different kinematical situation, the agreement is very good. This can be taken as additional proof that the parametrization of prefission and postfission neutrons obtained at 57° is indeed correct.

Concluding this section we point out two main results obtained from neutron emission in coincidence with FF products. The preequilibrium emission shows an increase with rising bombarding energy and the evaporative emission gives evidence for considerable neutron emission occurring before the composite system fissions.

IV. DISCUSSION AND COMPARISON WITH MODELS

A. Evaporative emission of neutrons in coincidence with ER and FF fragments

The evaporation of neutrons from the ER and the FF products of $^{165}\mathrm{Ho}+{}^{20}\mathrm{Ne}$ at bombarding energies from 220 to 402 MeV was calculated using the statistical model code JULIAN.[25] For nuclei at high spins the rotating-liquid-drop model[24] (RLDM) predicts similar deformation for the saddle point shape and the ground state shape. Assuming that fission is dominant in the high-spin region, we used the same level-density parameter a to calculate the probability for fission and evaporation. The fission barrier was set to the RLDM value and the code allowed the emission of n, p, d, t, α, and ^{6}Li particles using the level density formalism of Lang[26] with $a = A/8$. The excitation of the compound nucleus ^{185}Ir was lowered by the amount $M_{\mathrm{PE}}(S_n + \frac{3}{2}T_{\mathrm{PE}})$ to account for the measured preequilibrium emission of neutrons. However, no corrections for charged-particle preequilibrium emission were applied.

In Fig. 11 neutron energy spectra are shown which were measured at various angles in coincidence with ER. The results of JULIAN are represented by full lines. The calculated neutron multiplicities (given in parentheses) are higher than the measured ones: (9.9) 6.7 ± 0.5, (11.8) 8.4 ± 0.6, and (14.2) 10.1 ± 0.6 at 220, 292, and 402 MeV, respectively. Part of this discrepancy is probably due to the fact that we neglected charged particle preequilibrium emission and incomplete fusion. These effects would lower the excitation energy. In addition we did not consider the influence of temperature and deformation on the transmission coef-

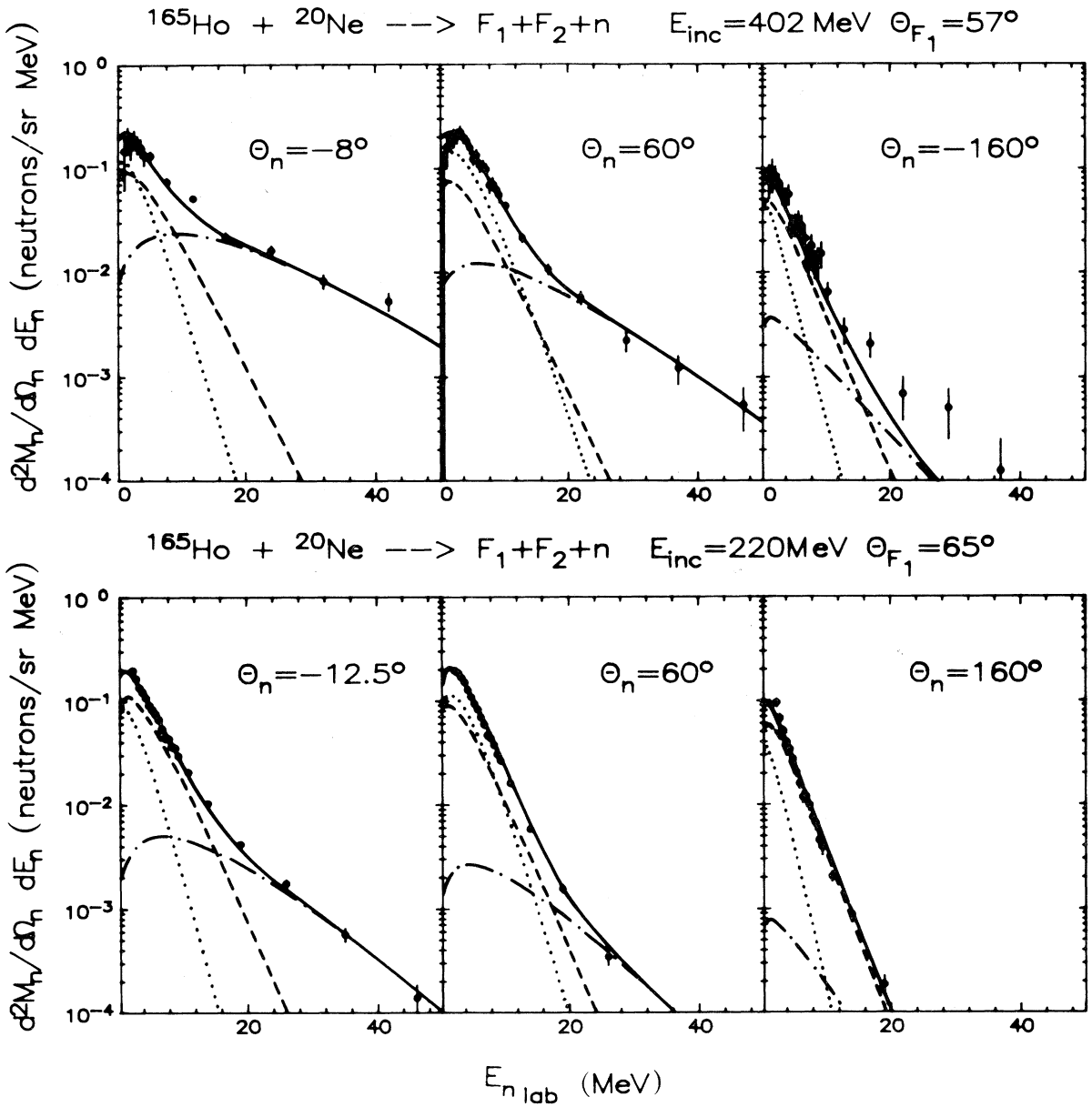

FIG. 9. Experimental differential neutron multiplicities in coincidence with one FF fragment at the 220 and 402 MeV bombarding energies (data points). Solid lines denote the calculation of the experimental spectra with Eq. (1) using four sources and the parameters from Table III. The dashed line corresponds to the evaporative prefission component, the dotted line to the evaporation from both fission fragments (postfission emission), and the dashed-dotted line to the preequilibrium component.

ficients for the evaporated particles. These effects could increase the ratio between the multiplicities of charged particles and neutrons.

For neutrons in coincidence with FF fragments the experimental results for the number of neutrons emitted before the composite system fissioned, and the deduced temperature of this system, can be used to estimate the time needed to emit those neutrons. This time will give us the information of how long the composite system has lived before it fissioned. The empirical formula by Stokstad,[27]

$$t_n = \langle M_n \rangle 0.5 \exp(13/\langle T \rangle) \times 10^{-22} \text{ s} , \quad (2)$$

using the prefission values for $\langle M \rangle$ and $\langle T \rangle$ from Table III gives $t = 4.2 \times 10^{-20}$, 2.6×10^{-20}, and 2.3×10^{-20} s for the 220, 292, and 402 MeV bombarding energies, respectively.

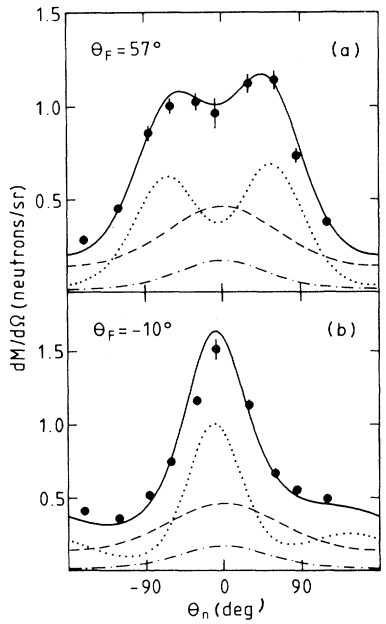

FIG. 10. The experimental angular correlation distribution of neutrons in coincidence with one FF fragment at the 402 MeV bombarding energy (data points). The upper part (a) is obtained for $2 \leq E_{n\,\mathrm{lab}} \leq 10$ MeV at $\theta_{FF} = 57°$. The lines denote the corresponding calculations using the least-squares fit parameters from Table III and the symbols for the curves are the same as in Fig. 9. The lower part shows the same angular correlation at a different triggering angle of $-10°$.

Before we compare the experimental result for the prefission neutron multiplicity and the calculation obtained by JULIAN, let us consider which processes contribute to prefission and postfission neutron emission. The colliding system passes from initial contact to the phase of fully accelerated fission fragments through the following stages: (i) projectile and target form a dinuclear complex which rotates and sticks together for some time before the compound nucleus is formed; (ii) the compound nucleus forms; (iii) the system passes over the saddle point, forms a neck and reaches scission, when the neck ruptures; and (iv) the two fragments are accelerated in their mutual Coulomb field to their asymptotic final kinetic energies. The system may emit particles in each of these stages, if the corresponding lifetime is long enough to allow particle emission.

The number of neutrons determined experimentally as emitted prior to fission contains contributions from all stages (i) to (iii) and a certain fraction of (iv). Namely, as long as the velocity of accelerating fission fragments $v_{FF}(t)$ is smaller than the velocity of the composite system V_{CM}, neutrons emitted from those fragments will be considered experimentally as prefission neutrons. As in our case V_{CM} is very small, ≈ 0.5 cm/ns, the time needed for fission fragments to gain this velocity is very short, $\approx 10^{-21}$ s, as calculated by assuming two spheres which are accelerated in their mutual Coulomb field and having zero relative energy at the moment of separation. The angular correlation of evaporated neutrons calculated as a function of kinetic energy of accelerating fission fragments can also show after which kinetic energy of fission fragments the neutron angular correlation becomes sufficiently distinguishable from the compound-nucleus neutron angular correlation.

In Fig. 12 we show the neutron angular correlation calculated for the 402 MeV bombarding energy and various kinetic energies of fission fragments ranging from zero to a maximum value reached in the Coulomb field. We find that for kinetic energies of fission fragments larger than ≈ 40 MeV corresponding to an acceleration time of 10^{-21} s the calculated neutron angular correlation becomes double peaked and well distinguished from the angular correlation of the prefission composite system. This figure should be compared with the experimental neutron angular correlation (Fig. 10). While the experimental value for the prefission neutron multiplicity covers several stages in the evolution of the dinuclear complex, the statistical model calculation considers only neutrons emitted from the compound nucleus stage (ii), as prefission neutrons. Using the input parameters as already described, the calculation performed by JULIAN gives $M_{PF} = 1.2$, 1.6, and 2.0 for 220, 292, and 402 MeV, respectively. We recall that the prefission multiplicity M_{PF}, determined by the analysis of the experimental spectra was ≈ 5.6 independent of the excitation energy. We mention that the calculated number of prefission neutrons could be increased to $M_{PF} = 3.6$, 5.4, and 7.4 using $a_f/a_n = 0.95$ and lowering the RLDM fission barrier by a factor of 0.75. However, if we assume that the saddle point shape has a lower symmetry than that of the ground state, the ratio a_f/a_n should be greater than 1.

If the statistical-model calculation with parameters based on the RLDM gives a reliable description of the compound-nucleus emission at such high excitation energies and angular momenta, we conclude that approximately four prefission neutrons are not accounted for by the compound nucleus emission. This also leads to the conclusion that, even at such high excitation energies and angular momenta, fission is quite a slow process. Similar evidence for large and constant prefission multiplicity for low-fissile nuclei ($A \approx 170$) at excitation energies above 135 MeV has also been reported by Gavron *et al.*[4] There are also indications of considerable proton

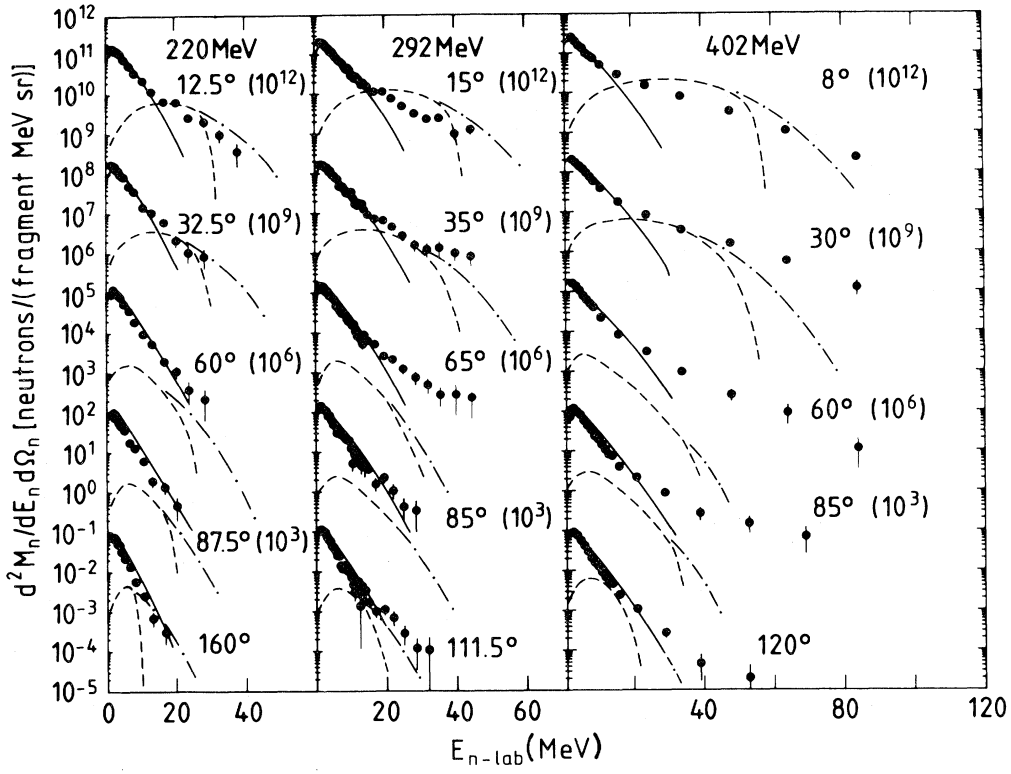

FIG. 11. Neutron spectra in coincidence with ER ($\theta_{ER}=8°$, 16°, and 10°) at the 220, 292, and 402 MeV bombarding energies. Data points: the experimental spectra in the laboratory system. Solid lines denote the calculations with the code JULIAN (Ref. 25); the dashed and dashed-dotted lines are the calculations with the Fermi-jet model (Ref. 12) using hard and soft ($T=3$ MeV) Fermi surfaces, respectively.

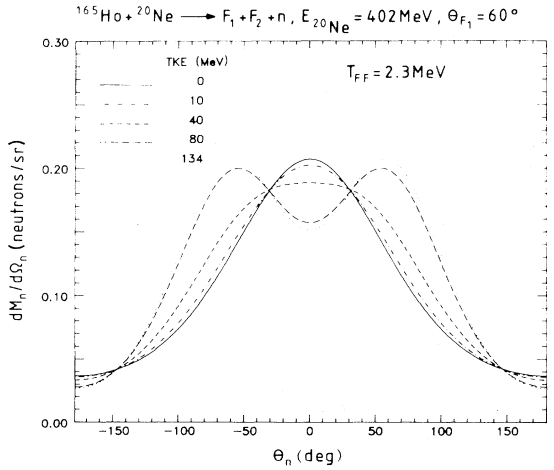

FIG. 12. Angular correlation calculated for neutrons evaporated from fission fragments at the 402 MeV bombarding energy and various kinetic energies of fission fragments (TKE) at the moment of emission. One fission fragment is emitted at $\theta_{F_1}=60°$; the temperature of each fission fragment is 2.3 MeV.

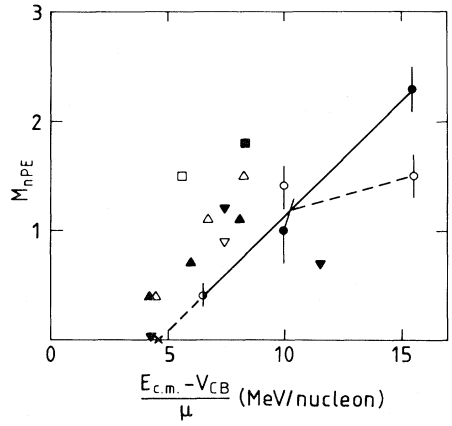

FIG. 13. Mean preequilibrium neutron multiplicity in coincidence with fusionlike events as a function of $(E_{c.m.}-V_{CB})/\mu$. Data points: Δ (^{157}Gd + ^{13}C), ▲ (^{158}Gd + ^{12}C), Ref. 5; □ (^{154}Sm + ^{16}O), Ref. 39; ■ (^{158}Gd + ^{12}C), x (^{150}Nd + ^{20}Ne), Ref. 38 (all data were from coincidences with ER); ∇ (^{150}Nd + ^{20}Ne→ER), ▼ (^{158}GD + ^{12}C and ^{150}Nd + ^{20}Ne→FF), Ref. 14; ○ (^{165}Ho + ^{20}Ne→ER), ● (^{165}Ho + ^{20}Ne→FF), present data. The solid and dashed lines are drawn through the present data points.

and alpha particle emission before fission for $^{12}C+^{197}Au$ and $^{12}C+^{251}Th$ systems at 30—60 MeV/nucleon[28] and for $^{20}Ne+^{197}Au$ at 20 MeV/nucleon (Ref. 29).

Possible reasons for an enhancement of neutron evaporation prior to fission were treated in a preliminary discussion by Britt and Gavron.[30] We will limit our discussion mainly to time estimates of various stages from fusion to fission.

We have to ask how long ^{165}Ho and ^{20}Ne nuclei initially stay in the phase of a dinuclear molecule and what amount of time they need to drift to mass asymmetry (compound nucleus). According to trajectory calculations including the neck degree of freedom,[31] the formation of a compound nucleus in the system $^{165}Ho+^{20}Ne$ seems to be a very fast process, lasting $\approx 10^{-22}$ s. This time would not be long enough to enable any particle evaporation from this stage.

Furthermore, we can ask how long a system like ^{185}Ir needs to go from saddle to scission. Such low-fissile systems in which the saddle point shape is very close to the scission configuration have not very often been investigated. According to the liquid-drop theory, assuming an irrotational nonviscous incompressible fluid,[32] the saddle-to-scission transition time for a system with fissility $x \approx 0.66$ and zero spin would be of the order of 1.5×10^{-21} s. This time also is not long enough to evaporate ≈ 4 neutrons. For high spins, however, the shape will become more compact, which would tend to increase the saddle-to-scission transition time whereas the centrifugal force would tend to decrease this time. Thus we assume that the two opposing effects cancel each other. However, the saddle-to-scission transition time is not a well known quantity even for small angular momenta. Systems like ^{236}U have been very extensively studied experimentally and theoretically. According to the same theory[32] mentioned before ^{236}U should have saddle-to-scission transition times (t_{ss}) approximately two times larger than ^{185}Ir,

$$t_{ss}=2.8\times 10^{-21}\ \text{s} .$$

There are, however, various estimates[33] for t_{ss}, predicting times even larger than 10^{-20} s.

By increasing the viscosity of the system,[34,35] transition times of $\approx 5\times 10^{-21}$ s are obtained. The one-body dissipation mechanism leads also to longer saddle-to-scission transition times,[36] being of the order of 10^{-20} s. The information about the viscosity of a system, and consequently, about saddle-to-scission transition times, can be obtained by measuring the most probable kinetic energy of fission fragments. Systematic information exists for systems at moderate excitation energies.[34] For lighter, less fissile systems, the most probable kinetic energy of fragments is not very sensitive to the change of the viscosity. The energy at the scission point determines also the saddle-to-scission transition time. An upper limit for ^{236}U seems to be about 8—10 MeV, but it could also be very small, ≈ 0.5—1 MeV.[37] Such low scission energies result in long saddle-to-scission transition times.

From the present investigation and the experimental evidence it does not seem possible to clearly answer the question: What is the reason for and what processes mainly contribute to high prefission multiplicities? The mass-asymmetry effects in the entrance channel should be reexamined experimentally and theoretically. It is also possible that at such high excitation energies the statistical models, so far employed, do not give the proper description of the energy dependence of fission and particle emission widths during deexcitation. How much time the system needs to pass from saddle to scission should also be reexamined. From various possible experimental methods to determine this time, measurements of the number of particles emitted (evaporated) from this stage could be a powerful tool. However, this method can be only applied at high temperatures ($T \geq 2$ MeV) where the time needed to evaporate a neutron is small compared to the saddle-to-scission transition time.

B. Preequilibrium neutron emission

1. Systematics of preequilibrium neutrons in coincidence with fusionlike products

Reliable information about the preequilibrium emission mechanism induced by heavy ions can be obtained only from selective coincidence experiments. We will summarize now some main features of the preequilibrium neutron emission observed by various groups from central heavy-ion collisions. In Refs. 3, 5, 14, 38, and 39 preequilibrium neutrons were detected in coincidence with ER, while preequilibrium emission in coincidence with FF products was reported in Refs. 3, 14, and 40. The number of neutrons emitted due to preequilibrium emission was in all these experiments determined by a similar parametrization [Eq. (1)] of high-energy tails of neutron spectra.

In Fig. 13 we show the number of preequilibrium neutrons as a function of center-of-mass energy per nucleon above the Coulomb barrier, obtained in all experiments mentioned above. Despite quite a scattering of experimental preequilibrium multiplicities obtained for various medium-heavy systems we could, nevertheless, trace an approximate linear in-

crease as the $E_{c.m.}$ energy per nucleon above the Coulomb barrier increases. The onset of preequilibrium emission is approximately at 4—6 MeV/nucleon.

Comparing the evaporation time and the nuclear relaxation time as a function of temperature we observe[21] that at temperatures of 6—8 MeV the time to evaporate a light particle becomes shorter than the nuclear relaxation time. If we associate the maximum local temperature with the energy per nucleon above the barrier, such temperatures of 6 to 8 MeV are reached at 7 to 8 MeV/nucleon. Thus, this nonequilibrated part of the interaction region will start to emit particles before it has reached equilibrium. This would be consistent with our observation that preequilibrium emission sets in at 4—6 MeV/nucleon above the barrier.

However, the exciton model[41] predicts the onset of preequilibrium emission at similar energies per nucleon also. In this model the condition for preequilibrium emission is that the excitation energy per initial exciton should be larger than the binding energy of the emitted particle. If we assume the number of initial excitons to be equal to the number of nucleons in the projectile we obtain 8.28 MeV/exciton for 220 MeV Ne on ^{165}Ho. This is again in agreement with our observation. More important, if we consider the fractional preequilibrium neutron multiplicity we observe that 6 (4) %, 14 (9) %, and 12 (10) % of all emitted neutrons in coincidence with ER (FI) at energies of 6.5, 10.1, and 15.5 MeV/nucleon, respectively, are emitted before the system reaches an equilibrium. Very similar results have been obtained for light-ion induced reactions.[42] For instance, West[43] observed that in the reaction ^{58}Ni(α,p) at an α energy of 42 MeV about 6% of the total number of emitted protons are preequilibrium protons. This α energy corresponds to the 45 MeV excitation energy, or 7.5 MeV/nucleon above the barrier. This interesting similarity with the neon-induced reaction at the 220 MeV bombarding energy, corresponding to 165 MeV excitation energy or 6.5 MeV/nucleon above the barrier, has two consequences. First, it seems to indicate that not the total excitation energy is the important quantity to classify the occurrence of preequilibrium emission, but rather that the energy per nucleon above the barrier[21] or the initial relative velocity of the interacting nuclei. Second, the energy per nucleon enables us to directly compare preequilibrium light particle emission induced by light and heavy ions.

However, none of these models predicting the onset of preequilibrium particle emission consider the angular momenta. And indeed in our data, shown in Fig. 13, there is no difference at the two lower bombarding energies between preequilibrium neutrons from ER and FF fragments. The respective l ranges leading to ER and FF are 0—64$\hbar$ and 65—104$\hbar$. However, at the highest bombarding energy we observe a saturation of M_{PE} for ER whereas that for FF continues to rise. This observation could rule out several models which completely neglect the angular momentum brought into the system. Furthermore, it would also indicate that the mechanism is more likely related to the angular momentum limitation of complete fusion.[39,44] However, the difference of M_{PE} observed for ER and FF fragments could also simply be due to the fact that at 402 MeV we have a third heavy PL particle from a massive transfer reaction in the exit channel. In this case the third heavy particle can emit sequentially neutrons having in the laboratory system high energies since they are emitted from a source moving with 6—10 MeV/nucleon. That is, we would erroneously identify these sequentially evaporated neutrons as preequilibrium particles, whereas for the ER we have used the velocity of ER to ensure that such processes do not contribute.

2. *Hot moving source?*

In this subsection we would like to comment on the physical meaning of the parameters (given in Tables II and III) obtained from the multiple-source fit using Eq. (1). The parameters obtained in such a way, though mostly from inclusive data, are often interpreted in the literature as the parameters of a hot moving source.[4,45] The fact that the velocity of the source is approximately half the velocity of the projectile is used as a strong indication that only a subsystem of two times the nucleons of the projectile make up the hot source. Using the relation $A = E^*_{PE} 8 / T_{PE}{}^2$ we obtain also numbers close to 40, namely, 35 (32), 42 (35), and 27 (37) for ER (FF) at the 220, 292, and 402 MeV bombarding energies. The respective source velocities are 0.6 (0.5), 0.4 (0.5), and 0.5 (0.4) times the beam velocity. Despite these apparent successes we are very skeptical about relating T_{PE} and ϵ_{PE} to a temperature and a velocity of a hot source. The reason for this is mainly the fact that the extracted temperature depends very strongly on the angles used in the fit. For instance, if one extracts a temperature for each angle one gets a decreasing temperature with increasing neutron angle.

Starting from a conceptually similar model of a moving source inside the nucleus, Brosa *et al.*[46] have treated this problem by employing quantum mechanics instead of thermodynamics. They treat the time evolution of a wave packet which has an initial velocity v_0 and a spatial width σ_0 inside the nucleus. Varying these parameters Brosa *et al.* have

fitted our ER data and they obtain for the initial velocity of the wave packet 0.26, 0.26, and 0.36 times the beam velocity for bombarding energies of 220, 292, and 402 MeV, respectively. The spatial width can be translated into a momentum width $\sigma_p = \hbar/2\sigma_0$. For the respective spatial width (momentum width) Brosa *et al.* obtain 1.45 (68 MeV/c), 1.30 (76 MeV/c), and 1.11 fm (89 MeV/c) at 220, 292, and 402 MeV. Comparing the velocities obtained by these two models one reaches significantly different conclusions. This seems to be another indication that one should not use the parameters obtained literally and associate them with a physical meaning.

3. Comparison with the Fermi-jet model

The Fermi-jet model or the model of promptly emitted particles[12] (PEP) describes the emission of highly energetic particles from colliding heavy ions by the coupling between the relative velocity of the two interacting heavy ions and the intrinsic Fermi velocity. Owing to the long mean free path length of nucleons in cold nuclei most particles pass freely without any collision through the window opened up between the colliding nuclei and through the recipient nucleus (one-body PEP), whereas the contribution from particles having undergone any collisions is very small[12] (two-body PEP, etc.). The dashed lines in Fig. 11 show the calculated neutron spectra at various angles and at the 220, 292, and 402 MeV bombarding energies using the one-body PEP model.[12]

The calculations were performed using $l \leq l_{\text{crit}}^{\text{ER}} = 60\hbar$, where $l_{\text{crit}}^{\text{ER}}$ is determined from our experimental data for the ER cross section. Furthermore, we assumed a zero temperature Fermi distribution with a Fermi energy of 37 MeV. The one-body PEP model underestimates the highest particle energies, as well as the emission at larger angles ($\theta_n > 30°$). If a soft Fermi surface is used with a temperature of 3 MeV, the agreement at higher neutron energies considerably improves (dashed-dotted line in Fig. 11). However, the too strong focusing into the forward direction remains. The inclusion of many-body PEP's, i.e., of several nucleon-nucleon collisions before emission, would produce more particles emitted at larger angles and therefore improve the description of angular distribution. Furthermore, the PEP model predicts also an enhanced emission to the most backward angles (backward PEP) which is a unique feature of this model. It is hard to distinguish experimentally, however, this emission from the dominant compound-nucleus evaporation. On the basis of the angular distribution we have to conclude that the one-body PEP model is not able to reproduce the measured energy spectra.

4. Comparison with the modified Harp-Miller-Berne model

The original Harp-Miller-Berne model[47] describes the emission during relaxation in high-energy nuclear reactions using the Boltzmann master equation. This model was also applied to the preequilibrium emission in light-ion induced reactions at lower excitation energies[48] (a few tens of MeV). A master equation approach is used to describe the preequilibrium emission within the exciton model.[42] Blann[11] recently modified the Harp-Miller-Berne model in order to treat heavy ions as projectiles, too.

The model considers only s-wave collisions. In its present form it does not consider the angular distribution of emitted particles and only the emission of neutrons and protons is calculated. The model contains two free parameters: the scaling factor for the intranuclear transition rates and the initial degree of freedom n_0 (exciton number). The calculation performed in this work used the same scaling factor of 0.5 as suggested by Blann.[11] However, the use of scaling factors from 1 to 0.1 did not considerably change the calculated spectra. The slope of the

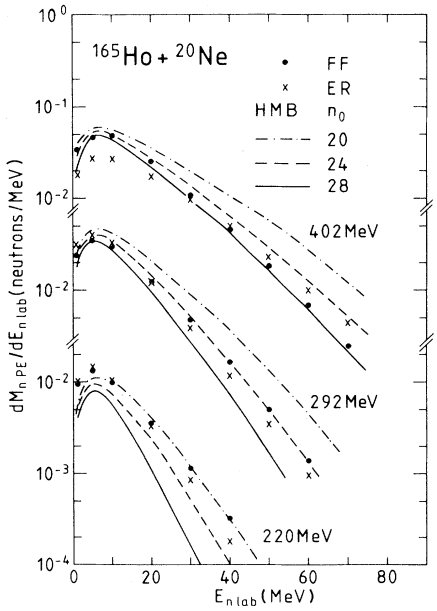

FIG. 14. Angle integrated preequilibrium neutron spectra in coincidence with ER and FF products at three bombarding energies ($\times$ and filled circles), compared with the calculation (curves) obtained with the modified HMB model (Ref. 11) using various n_0 values. For comparison with the calculation the data points have been divided by 2.

spectra is most sensitive to the n_0 value.

We wanted to compare only the preequilibrium emission of neutrons in our experiments with the modified Harp-Miller-Berne (HMB) model.[11] In order to obtain the angle-integrated preequilibrium neutron spectra from our experimental data we use the multiple-source fit. The angle-integrated spectra at all bombarding energies for ER- and FF-neutron-coincidence data are calculated using the parameters M_{PE}, T_{PE}, and ϵ_{PE} from Tables II and III.

We show in Fig. 14 the calculation at all three bombarding energies using $n_0=20$, 24, and 28. The preequilibrium spectra of neutrons in coincidence with ER and FF products are very well described with the modified HMB model using $n_0=20$ at 220 MeV and $n_0=24$ at 292 MeV. The results at 402 MeV for FF data are well reproduced by the same model using $n_0=28$. The preequilibrium neutron spectra in coincidence with ER at the last bombarding energy differ somewhat in shape from the FF data. This was already observed by fitting the spectra (Tables II and III). The modified HMB model does not reproduce so nicely the "experimental" data with any n_0, but nevertheless, the values between $n_0=24$ and 28 can be applied. We conclude that the modified HMB model gives an overall good description of the experimental preequilibrium neutron spectra if n_0 varies with the bombarding energy. Using the scaling factor of 0.5 as described previously, the calculated spectra underestimate the data by approximately a factor of 2. At bombarding energies close to the onset of preequilibrium emission, the initial degree of freedom seems to be defined by the projectile nucleons alone. As the bombarding energy increases, additional degrees of freedom have to be taken into account.

The same model was recently applied also to the emission of protons in ^{16}O-induced reactions[49] where the same energy dependence of the n_0 parameter was observed. The comparison of neutron spectra with the modified HMB model reported by Gavron *et al.*[5] indicates similar conclusions. It seems to be a general finding that the initial degree of freedom is an energy-dependent quantity. This effect was not observed in light-ion induced reactions.

V. CONCLUSION

In summary, the most interesting results of this investigation of the neutron emission in central Ho + Ne collisions are (i) the onset and energy dependence of the preequilibrium neutron emission, and (ii) the high prefission neutron multiplicity. Experimentally it is found that in central collisions of Ho + Ne between 5 and 15 % of the total number of emitted neutrons are emitted before the system reaches a thermal equilibrium. Furthermore the preequilibrium neutron emission sets in at about 5 to 6 MeV/nucleon above the Coulomb barrier and is increasing with the bombarding energy. The results are very similar for ER and FF events though only for the ER did the measured velocity of the evaporation residues make it possible to discriminate between almost full and incomplete linear-momentum transfer. With the increasing preequilibrium neutron emission the temperature, as measured with the evaporated neutrons, decreases from almost 100% of the calculated value, assuming that all the excitation energy went into internal excitation energy at the lowest bombarding energy, to about 80% at the two higher bombarding energies.

The comparison of the measured neutron energy spectra with various models has given no conclusive result for the physical process which is producing the preequilibrium neutrons. The Fermi-jet model can describe the energy spectra reasonably well at small angles only, if one assumes a soft Fermi surface. This model fails completely in predicting the high-energy component at large angles, a failure which could, however, be overcome if one would also take into account multiple scattering of the Fermi-jet nucleons prior to emission. In this case the Fermi-jet model becomes essentially an intranuclear cascade model. The modified Harp-Miller-Berne model can describe very well the angle-integrated energy spectra; however, the initial degree of freedom n_0 is increasing with the bombarding energy, which is not understood quantitatively. Qualitatively, one could ascribe this increase of n_0 to the increasing contribution of collective degrees of freedom. Machner[50] has compared our results with the exciton model of Mantzouranis and Weidenmüller,[51] which also calculates angular distributions. He gets good agreement with the measured energy spectra at all angles. The multiple source fit of the preequilibrium component results in parameters which, if associated to a "temperature" and a source velocity, agree with the picture of a hot moving source. However, it is not clear whether this agreement is merely accidental. The fact that, if one extracts a temperature for different angles, one obtains an angle-dependent temperature, is especially conceptually difficult to understand.

The second interesting finding of the present investigation is the unexpectedly high prefission neutron multiplicity of about 5.6 neutrons independent of the bombarding energy, whereas the expectation from the statistical model is only 1.5 to 2 prefission neutrons. Although we cannot give a unique explanation for this finding, it seems most likely that the main reason for this high prefission neutron

multiplicity is a very slow transition from saddle to scission. The other possible reasons for such a high prefission neutron multiplicity are a very slow mass asymmetry relaxation time, a hindrance of the collective degree of freedom leading to the fission path, wrong level densities used in the statistical model at high excitation energies and angular momenta, and finally the possibility of a considerable neutron emission during the neck rupture. For a better understanding of the high prefission neutron multiplicity it is necessary to study, for instance, the entrance channel effect. This will make it possible to decide whether the fusion or the fission dynamics cause the high prefission neutron multiplicity.

---

*On leave from the Rudjer Bošković Institute, Zagreb, Yugoslavia.

[1]W. U. Schröder and J. R. Huizenga, Annu. Rev. Nucl. Sci. 27, 465 (1977).

[2]W. U. Schröder, in *Proceedings of the International Symposium on Continuum Spectra of Heavy Ion Reactions, San Antonio, 1979,* edited by T. Tamura, J. B. Natowitz, and D. H. Youngblood (Harwood, New York, 1980), p. 19.

[3]D. Hilscher, E. Holub, U. Jahnke, H. Orf, and H. Rossner, in *Dynamics of Heavy-Ion Collisions,* Proceedings of the Third Adriatic Europhysics Study Conference, Hvar, Yugoslavia, 1981, edited by N. Cindno, R. A. Ricci, and W. Greinen (North-Holland, Amsterdam, 1981), p. 225.

[4]D. K. Scott, see Ref. 3, p. 241.

[5]A. Gavron, J. R. Beene, R. L. Ferguson, F. E. Obenshain, F. Plasil, G. R. Young, G. A. Petitt, K. Geoffroy Young, M. Jääskeläinen, D. G. Sarantites, and C. F. Maguire, Phys. Rev. C 24, 2048 (1981).

[6]R. P. Schmitt, G. J. Wozniak, G. U. Rattazzi, G. J. Matthews, R. Regimbart, and L. G. Moretto, Phys. Rev. Lett. 46, 522 (1981).

[7]C. K. Gelbke, M. Bini, C. Olmer, D. L. Hendrie, J. L. Laville, J. Mahoney, M. C. Mermaz, D. K. Scott, and H. H. Wieman, Phys. Lett. 71B, 83 (1977).

[8]M. Bini, C. K. Gelbke, D. K. Scott, T. J. M. Symons, P. Doll, D. L. Hendrie, J. L. Laville, J. Mahoney, M. C. Mermaz, C. Olmer, K. Van Bibber, and H. H. Wiemann, Phys. Rev. C 22, 1945 (1980).

[9]J. W. Harris, T. M. Cormier, D. F. Geesaman, L. L. Lee, Jr., R. L. McGrath, and J. P. Wurm, Phys. Rev. Lett. 38, 1460 (1977).

[10]M. B. Tsang, W. G. Lynch, R. J. Puigh, R. Vandenbosch, and A. G. Seamster, Phys. Rev. C 23, 1560 (1981).

[11]M. Blann, Phys. Rev. C 23, 205 (1981).

[12]J. P. Bondorf, J. N. De, G. Fai, A. O. T. Karvinen, B. Jakobssen, and J. Randrup, Nucl. Phys. A333, 285 (1980).

[13]C. Gregoire, C. Ngô, and B. Remaud, Phys. Lett. 99B, 17 (1981).

[14]A. Gavron, J. R. Beene, B. Cheynis, R. L. Ferguson, F. E. Obenshain, F. Plasil, G. R. Young, G. A. Petitt, M. Jääskeläinen, D. G. Sarantites, and C. F. Maguire, Phys. Rev. Lett. 47, 1255 (1981); 48, 835(E) (1982).

[15]R. A. Cecil, B. D. Anderson, and R. Madey, Nucl. Instrum. Methods 161, 439 (1979).

[16]R. E. Textor and V. V. Verbinski, Oak Ridge National Laboratory Report No. ORNL-4160, 1968 (unpublished).

[17]M. Drosg, Nucl. Instrum. Methods 105, 573 (1972).

[18]K. H. Maier and J. Nitschke, Nucl. Instrum. Methods 59, 227 (1968).

[19]H. R. Bowman, S. G. Thompson, J. C. D. Milton, and W. J. Swiatecki, Phys. Rev. 126, 2120 (1962).

[20]H. O. Neidel and H. Henschel, Nucl. Instrum. Methods 178, 137 (1980).

[21]D. Hilscher, J. R. Birkelund, A. D. Hoover, W. U. Schröder, W. W. Wilcke, J. R. Huizenga, A. C. Mignerey, K. L. Wolf, H. F. Breuer, and V. E. Viola, Phys. Rev. C 20, 576 (1979).

[22]K. J. Le Couteur and D. W. Lang, Nucl. Phys. 13, 32 (1959); D. W. Lang, *ibid.* 53, 113 (1964).

[23]H. Rossner, D. Hilscher, E. Holub, G. Ingold, U. Jahnke, H. Orf, J. R. Huizenga, J. R. Birkelund, W. U. Schröder, and W. W. Wilcke, Phys. Rev. C 27, 2666 (1983).

[24]S. Cohen, F. Plasil, and W. J. Swiatecki, Ann. Phys. (N.Y.) 82, 557 (1974).

[25]M. Hillman and Y. Eyal (unpublished).

[26]D. W. Lang, Nucl. Phys. 77, 545 (1966).

[27]R. G. Stokstad, in *Proceedings of the Topical Conference on Heavy-Ion Collisions, Falls Creek Falls State Park, Tennessee, 1977* (U.S. Department of Commerce, Washington, D.C., 1977).

[28]M. F. Rivet, B. Borderie, S. Song, D. Guerreau, H. Oeschler, R. Bimbot, I. Forest, J. Galin, D. Gardes, B. Gatty, M. Lefort, B. Tamain, and X. Tarrago, Nucl. Phys. A387, 143 (1982).

[29]Ch. Egelhaaf, M. Bürgel, H. Fuchs, A. Gamp, H. Homeyer, and D. Kovar, Hahn Meitner Institute Report No. HMI-83/4R (unpublished).

[30]H. C. Britt and A. Gavron, in *Proceedings of the International Symposium on Nuclear Fission and Related Collective Phenomena, Bad Honnef, 1981,* Lecture Notes in Physics 158, edited by P. David, T. Mayer-Kuckuk, and A. van der Woude (Springer, Berlin, 1982), p. 24.

[31]J. R. Huizenga, J. R. Birkelund, W. U. Schröder, W. W. Wilcke, and H. J. Wollersheim, see Ref. 3, p. 15; W. U. Schröder, private communication.

[32]J. R. Nix, Nucl. Phys. A130, 241 (1969).

[33]H. A. Nifencker, J. Blachot, J. P. Bocquet, R. Brissot, J.

Crancon, C. Hamelin, G. Mariolopoulos, and C. Ristori, in *Proceedings of the Symposium on the Physics and Chemistry of Fission, Jülich, 1979,* edited by J. W. Weil (IAEA, Vienna, 1980), Vol. II, p. 35.

[34]K. T. R. Davies, A. J. Sierk, and J. R. Nix, Phys. Rev. C 13, 2385 (1976).

[35]K. T. R. Davies, R. A. Managan, J. R. Nix, and A. J. Sierk, Phys. Rev. C 16, 1890 (1977).

[36]J. W. Negele, S. E. Koonin, P. Möller, J. R. Nix, and A. J. Sierk, Phys. Rev. C 17, 1098 (1978).

[37]C. R. Guet, H. A. Nifenecker, C. Signarbieux, and M. Asghar, see Ref. 33, Vol. II, p. 247.

[38]L. Westerberg, D. G. Sarantites, D. C. Hensley, R. A. Dayras, M. L. Halbert, and J. H. Barker, Phys. Rev. C 18, 796 (1978).

[39]K. Geoffroy Young, D. G. Sarantites, J. R. Beene, M. L. Halbert, D. C. Hensley, R. A. Dayras, and J. H. Barker, Phys. Rev. C 23, 2479 (1981).

[40]J. Kasagi, S. Saini, T. C. Awes, A. Galonsky, C. K. Gelbke, P. Poggi, D. K. Scott, K. L. Wolf, and R. L. Legrain, Phys. Lett. 104B, 434 (1981).

[41]M. Blann, Nucl. Phys. A235, 211 (1974).

[42]M. Blann, Annu. Rev. Nucl. Sci. 25, 123 (1975).

[43]R. W. West, Phys. Rev. 141, 1033 (1966).

[44]J. Wilczynski, K. Siwek-Wilczynska, J. van Driel, S. Ganggrijp, D. C. J. M. Hageman, R. V. F. Janssens, J. Lukasiak, and R. H. Siemssen, Phys. Rev. Lett. 45, 606 (1980).

[45]T. C. Awes, G. Poggi, C. K. Gelbke, B. B. Back, B. G. Glagola, H. Breuer, and V. E. Viola, Jr., Phys. Rev. C 24, 89 (1981).

[46]V. Brosa and W. Krone, Phys. Lett. 105B, 22 (1981).

[47]G. D. Harp, J. M. Miller, and B. J. Berne, Phys. Rev. 165, 1166 (1968).

[48]G. D. Harp and J. M. Miller, Phys. Rev. C 3, 1847 (1971).

[49]T. C. Awes, S. Saini, G. Poggi, C. K. Gelbke, D. Cha, R. Legrain, and G. D. Westfall, Phys. Rev. C 25, 2361 (1982).

[50]H. Machner, Phys. Lett. 86B, 129 (1979); private communication.

[51]G. Mantzouranis, H. A. Weidenmüller, and D. Agassi, Z. Phys. A 276, 145 (1976).